Supporting Information for

Studies of Cobalt-Mediated Electrocatalytic CO_2 Reduction Using a Redox-Active Ligand

David C. Lacy, Charles C. L. McCrory, Jonas C. Peters*

Joint Center for Artificial Photosynthesis, Division of Chemistry and Chemical Engineering, California Institute of Technology, Pasadena, CA 91125, United States

E-mail: jpeters@caltech.edu

Contents

Crystallography

General Methods. XRD data was collected on either a Siemens or Bruker three-circle diffractometer with a Smart 1K CCD detector using Mo Kα radiation (λ = 0.71073), performing ϕ-and ω-scans and cooled with an Oxford Cryosystems crystal cooling system. The structures were solved by direct methods and refined on F^2 by full-matrix least-squares techniques using SHELX program package2,3,4 and Olex2.[1,2]

Table S1. Crystal data and structure refinement for the cobalt complexes.

	[Co**N$_4$**]	[Co**N$_4$H**(MeCN)][BPh$_4$]	[Co^{II}**N$_4$H**(MeCN)][OTf][BPh$_4$]
formula	$C_{15}H_{21}CoN_4$	$C_{41}H_{45}BCoN_5$	$C_{42}H_{45}BCoF_3N_5O_3S$
FW	316.29	677.61	826.63
T (K)	100	100	100
crystal system	Monoclinic	Triclinic	Monoclinic
space group	*P* 2$_1$/*c*	*P*–1	*P* 2$_1$/*c*
a (Å)	19.366(3)	10.8505(6)	17.3997(12)
b (Å)	5.0144(7)	11.3972(6)	12.7606(8)
c (Å)	15.594(2)	14.1924(8)	18.5157(10)
α (deg)	90	84.438(3)	90
β (deg)	111.445(3)	77.625(3)	106.663(1)
γ (deg)	90	80.132(3)	90
Z	4	2	4
V (Å^3)	1409.4(3)	1685.66(16)	3938.4(4)
d_{calcd} (Mg/m^3)	1.490	1.335	1.394
Indep. Reflections	5894	25679	19028
R1	0.0344	0.0339	0.0359
wR2	0.1169	0.1249	0.0950
GOF	0.8319	0.9585	1.003

Computational Methods.

Geometry optimizations were performed on the crystal coordinates of [Co**N$_4$**] and [Co**N$_4$H**(MeCN)]$^+$ using the Gaussian03 package.[3] For each calculation, an unrestricted B3LYP hybrid functional was used with TZVP functional for cobalt atoms and 6-31$^+$g(d) for the other atoms. After optimization, a frequency calculation was performed to ensure that they are true minima. To obtain the open-shell singlet configurations, we performed a wavefunction stability calculation provided by Gaussian03 (key word "stable=opt").[4] This method creates a broken symmetry solution with separated alpha and beta spin manifolds.[5] To ensure that the open-shell singlet was indeed lowest in energy, the same calculation was performed but with a forced restricted solution.

Table S2. Additional bulk electrolysis results for CO_2 reduction with cobalt-**N$_4$H** complexes.

Conditions[(a)]	Electrode	Potential (V)	%F_{CO}	%F_{H2}	%F_T	ref
MeCN (0.04 M H_2O)	glassy carbon	-2.1	24	< 1	24	This work
MeCN (10 M H_2O)	glassy carbon	-2.1	45	30	75	This work
MeCN (2.8 M H_2O)	mercury	-1.4	12	1	13	6
MeCN (2.8 M H_2O)	mercury	-1.8	33	3	36	6
DMF (2.8 M H_2O)	mercury	-1.7	66	5	71	6
MeCN (0.4 M H_2O)	pyrolytic graphite*	-2	25	0	25	7

(a) Electrolyte was 0.1 M *n*Bu_4NClO_4 for Peters, 0.1 M Et_4NCl for Tinnemans, and *n*Bu_4NBF_4 for Che. Bulk electrolysis experiments were conducted in CO_2 saturated solvent. Potentials are vs. $FeCp_2$.

* Pyrolytic graphite was used to collect the cyclic voltammograms, though no comment was given as to the electrode used for CPE experiments.

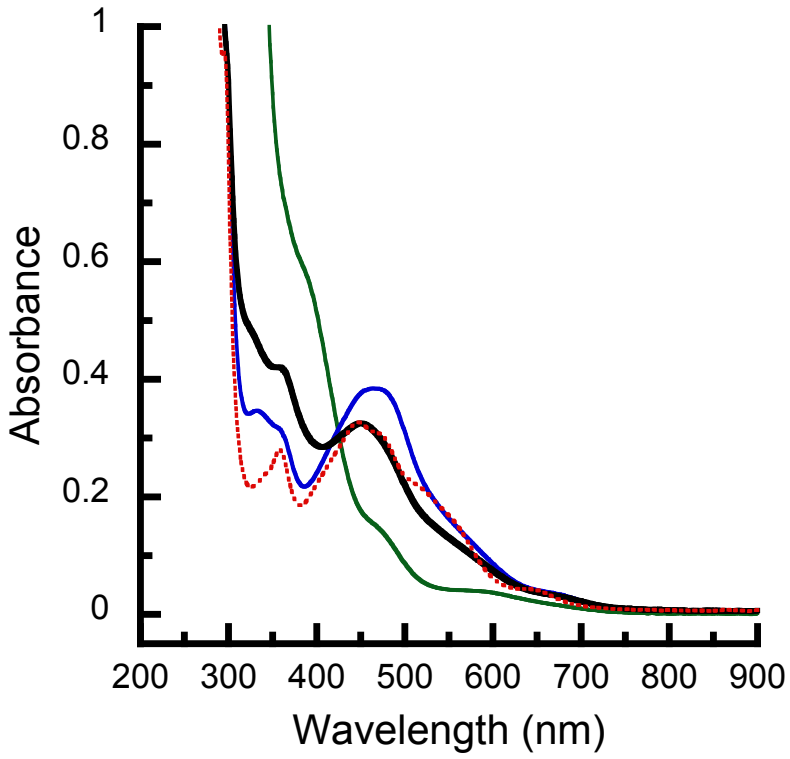

Figure S1. After a bulk electrolysis with 0.29 mM $[Co^{III}\mathbf{N_4H}(Br)_2]^+$ in CO_2 saturated MeCN with 10 M H_2O and 0.1 M nBu$_4$NClO$_4$, an aliquot from the working chamber was removed via cannula transfer into a CO_2 purged 1 cm UV-vis cuvette and a spectrum was collected (solid black). For comparison, the UV-vis spectrum of 0.31 mM $[Co^{II}\mathbf{N_4H}(Br)]^+$ (blue) and 0.29 mM $[Co^{III}\mathbf{N_4H}(Br)_2]^+$ (green) were collected under the same conditions (CO_2 saturated MeCN with 10 M H_2O, 0.1 M nBu$_4$NClO$_4$). The dashed red spectrum is $[Co^{II}\mathbf{N_4H}(MeCN)]^{2+}$ in neat MeCN normalized to a 0.27 mM concentration for comparison with the post CPE UV-vis spectrum.

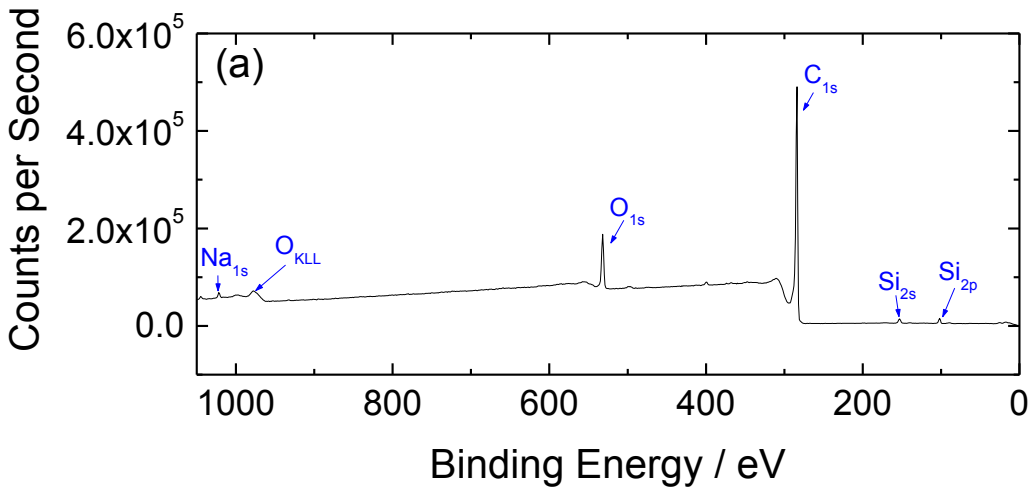

Figure S2. Representative XPS survey scans of a glassy carbon plate after a 40 minute electrolysis at -2.0 V (vs. $Ag/AgNO_3$ (1 mM)/MeCN reference electrode) in the presence of $[Co^{III}\mathbf{N_4H}(Br)_2]^+$ and CO_2. XPS and Auger peaks are assigned as labeled. The presence of Si is likely due to residual SiC from the pre-electrolysis polishing, and Ag is likely from electrodeposited Ag from small amounts of $AgNO_3$ leaking from the $Ag/AgNO_3$ (1 mM)/MeCN reference electrode during the 40-minute electrolysis. The small presence of Co on the surface is attributed to electrodeposited cobalt from the catalyst during the 40-minute bulk electrolysis experiment. Note that the Co 2p peaks are convoluted with the Co Auger signature,[8] making it difficult to quantify the amount of Co from this region. For that reason, the amount of Co was determined from the Co 3p peak as shown in Figure S3.

Table S3. XPS Atomic Percentages from fits of High-Resolution Scans.*

Element	Atomic % (Sample 1)	Atomic % (Sample 2)
C	89.28	89.81
O	8.60	8.95
Na	0.05	0.22
Si	1.99	0.76
Ag	0.03	0.02
Co	0.04	0.25
Fe	-	0.32[a]

*All atomic percentages were calculated from component fits from hi-resolution scans of individual XPS regions as shown in Figure S3. Note that the amount of Co was calculate from the Co 3p peak as shown in Figure S3(f). This is because the Co 2p peaks are convoluted with the Co Auger signature, making it difficult to quantify the amount of Co from this region.[6] The presence of Si is likely due to residual SiC from the pre-electrolysis polishing, and the presence of very small amounts of Ag is likely due to the electrodeposition of Ag from $AgNO_3$ leaking from the $Ag/AgNO_3$ (1 mM)/MeCN reference electrode during the 40 min electrolysis. The small amounts of Na are likely due to adsorption of trace Na impurities in the electrolyte. The Co signal is attributed to electrodeposited Co from the catalyst during the 40 min bulk electrolysis. [a]The Fe signal on sample 2 may be due to the electrodeposition of Fe from small amounts of $FeCp_2$ crossing through the fritted auxiliary chamber into the working chamber of the electrolysis cell

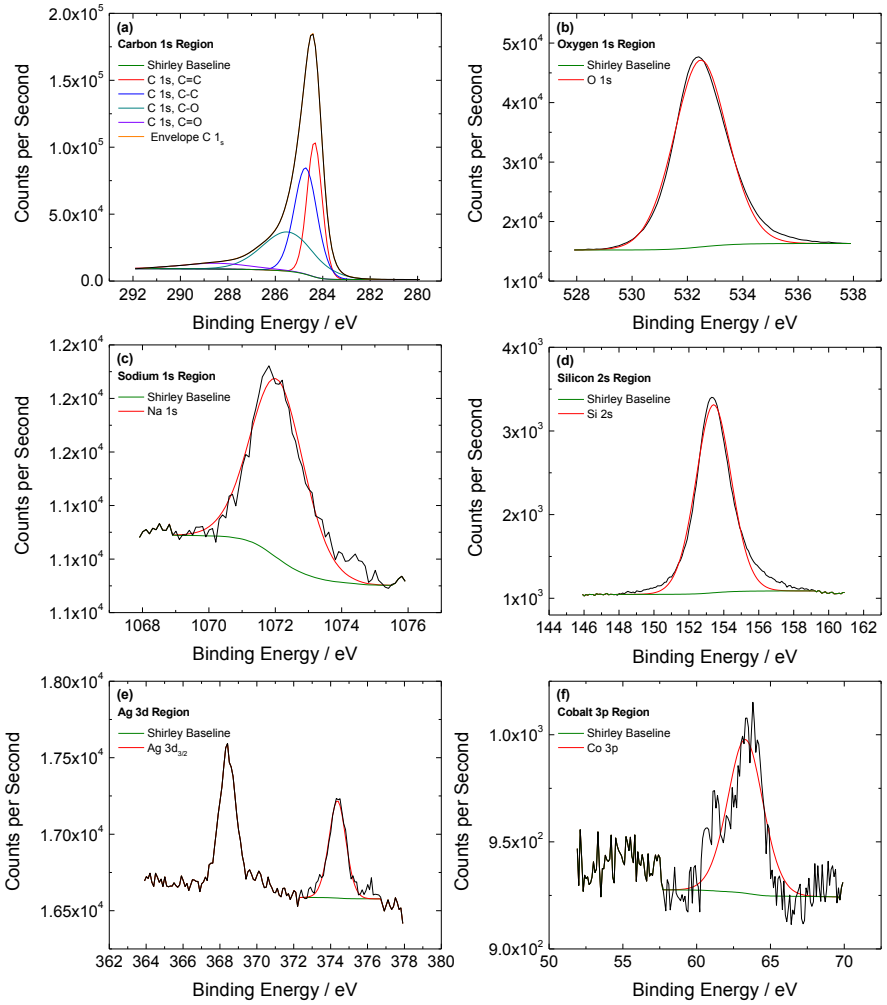

Figure S3. Representative high-resolution XPS scans of a glassy carbon plate after 40 min electrolysis at -2.0 V (vs. $Ag/AgNO_3$ (1 mM)/MeCN reference electrode) in the presence of $[Co^{III}\mathbf{N_4H}(Br)_2]^+$ and CO_2 in the (a) carbon 1s, (b) oxygen 1s, (c) sodium 1s, (d) silicon 2s, (c) silver 3d, and (f) cobalt 3p region. The component fits to each element in the corresponding XPS regions are shown as labeled in the figure. The carbon 1s peak in (a) was fit with the expected speciation in the C1s region.[9] The region in (f) was assumed to be due exclusively to Co 3p and contributions from possible Ag 4p and Na 2s peaks were not taken into account in the fitting—this gives us an upper limit for the amount of Co on the surface. The atomic percentages of each O, Na, Si, Ag, and Co were calculated from their respective component peaks in (b), (c), (d), (e), and (f) were normalized for their relative sensitivity factors. The atomic percentage of C was calculated from the region envelope area in (a) normalized to the C sensitivity factor. A table with all of the relevant data is shown in Table S3.

Table S4. Results of controlled potential electrolysis for electrocatalytic reduction of TsOH and [2,6-DCA][BF_4] with [$Co^{III}N_4H(Br)_2$]$^+$.*

Acid	[a] q / C	[b] f / %
CPE potential vs. $FeCp_2$		-1.01 V
TsOH	8 ± 1	87 ± 4
2,6-DCA	10 ± 2	87 ±11
CPE potential vs. $FeCp_2$		-1.21 V
TsOH	12 ± 3	86 ± 8
2,6-DCA	16 ± 1	90 ± 9

*Experiments were conducted in MeCN with 5.2 mM acid, 0.3 mM [Co^{III}**N_4H**$(Br)_2$]$^+$, 0.1 M $n$$Bu_4NClO_4$, glassy carbon working and counter electrode, $Ag/AgNO_3$(1 mM)/MeCN reference electrode with 0.1 M $n$$Bu_4NClO_4$ (externally referenced to the $FeCp_2^{+/0}$).[10] (a) q = charge; (b) f = Faradaic efficiency.

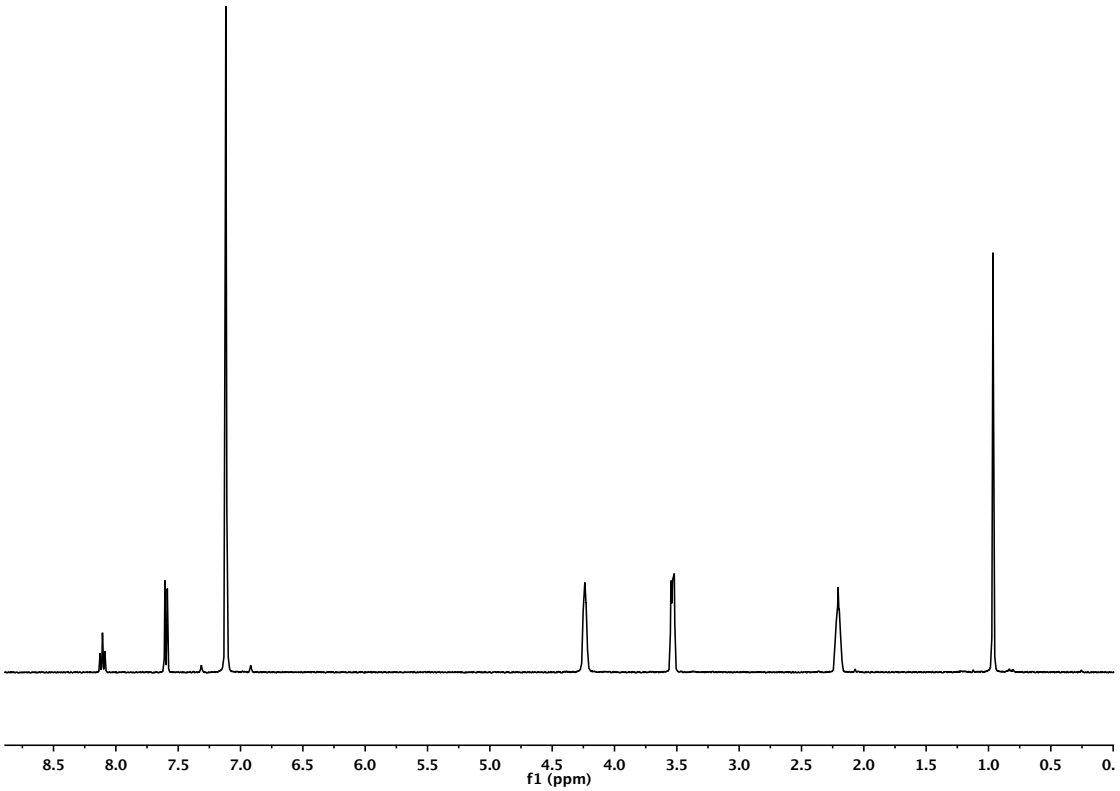

Figure S4. ^{1}H-NMR spectrum of [Co**N_4**] in C_6D_6.

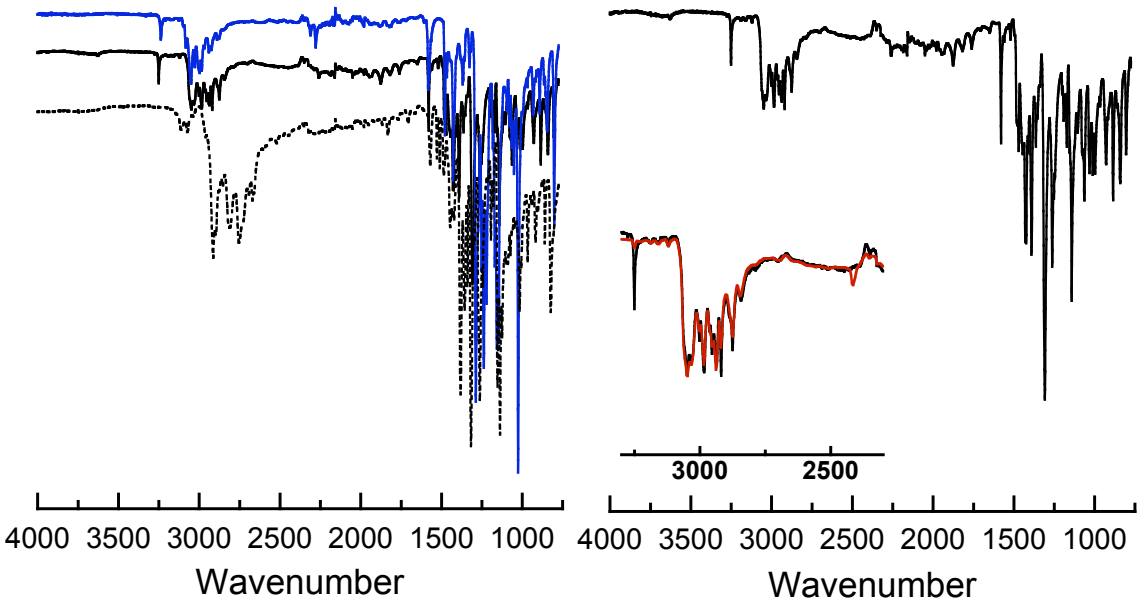

Figure S5. Left: FTIR-ATR spectra of [Co$\mathbf{N_4H}$(MeCN)][BPh_4] (solid black), [Co$\mathbf{N_4}$] (dashed black), and [$Co^{II}\mathbf{N_4H}$(MeCN)][OTf][BPh_4] (blue). Right: FTIR-ATR spectrum of [Co$\mathbf{N_4H}$(MeCN)][BPh_4] with inset showing isotopically sensitive peak upon deuterium labeling ([Co$\mathbf{N_4D}$(MeCN)][BPh_4] shown in red). The y-axis is in %-transmittance.

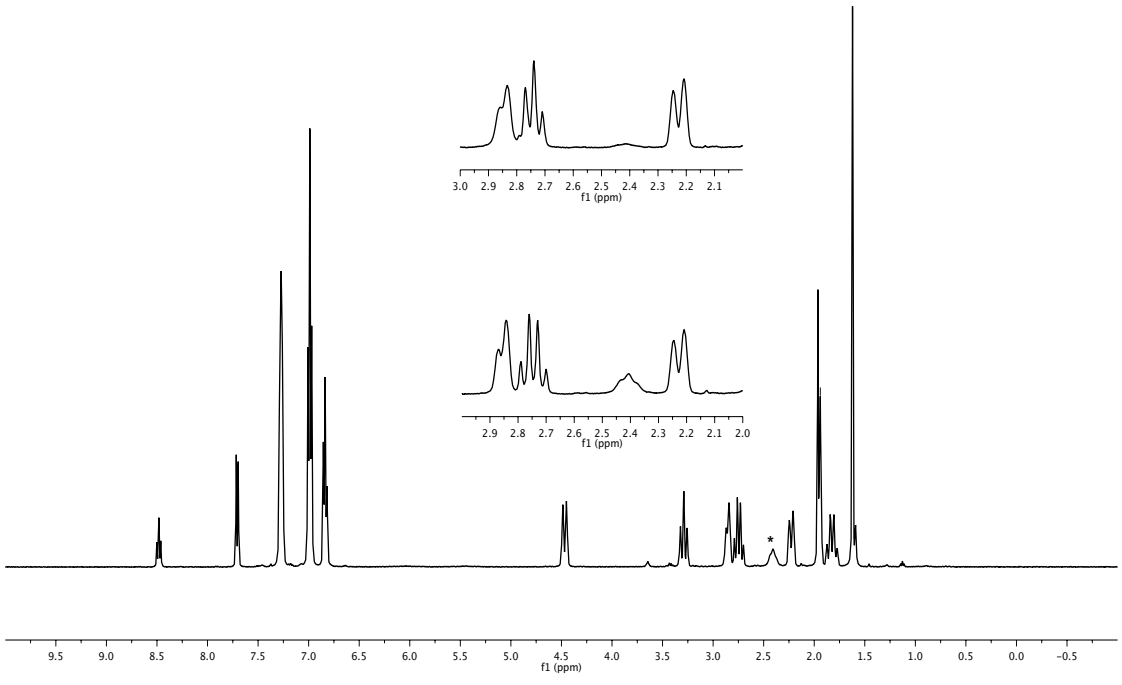

Figure S6. ^{1}H-NMR spectrum of [Co$\mathbf{N_4H}$(MeCN)][BPh_4] in MeCN-d_3. Asterisk indicates the NH resonance. The inset shows a zoomed view of the NH resonance (bottom inset) and the same view of the diminished resonance of [Co$\mathbf{N_4D}$(MeCN)][BPh_4] synthesized from D_2O (top inset).

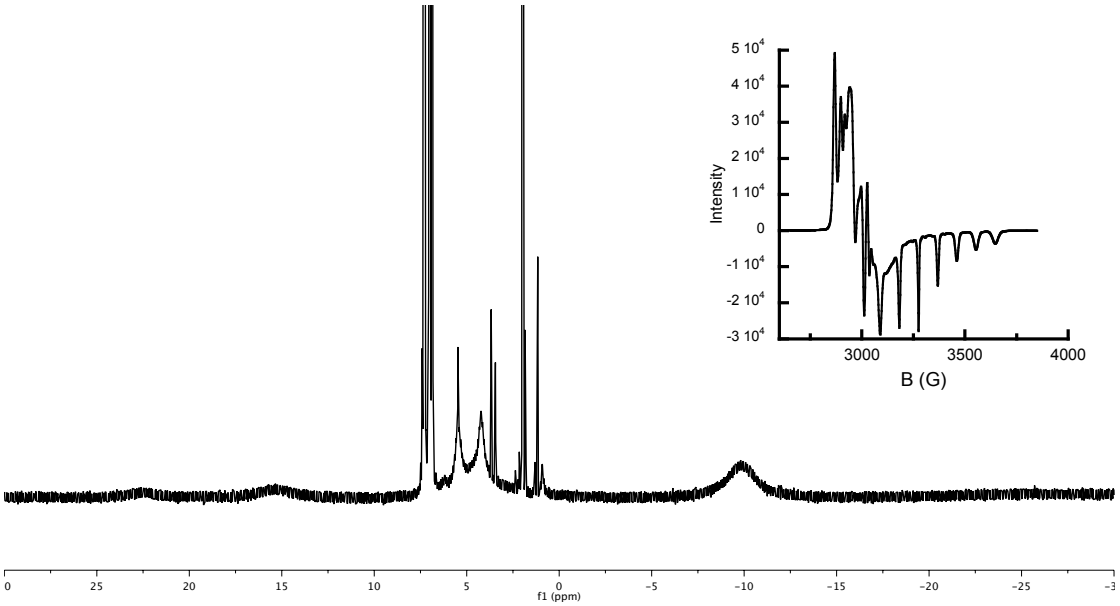

Figure S7. ^{1}H-NMR spectrum of analytically pure [Co^{II}**N$_4$H**(MeCN)][OTf][BPh$_4$] in MeCN-d_3. Inset: EPR spectrum of 15 mM sample of analytically pure [Co^{II}**N$_4$H**(MeCN)][OTf][BPh$_4$] in 50:50 DMF:THF mixture (conditions: # scans = 1; resolution = 1024 pts; sweep width 1200 G, Frequency, 9.397 GHz; Power = 2.041 mW, Mod. Freq. = 100.00 kHz; Mod. Amp. = 2.00 G; Conversion time = 163.840 ms; Time Constant = 40.960 ms; Sweep Time = 167.772 s).

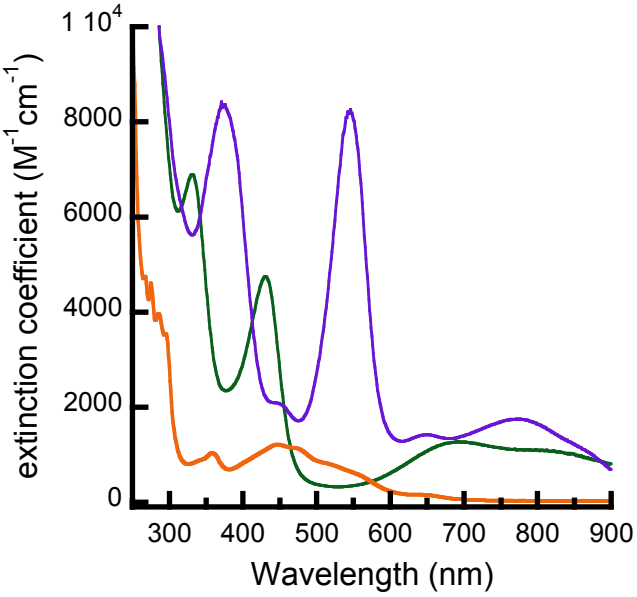

Figure S8. UV-vis spectrum of [Co**N$_4$**] in THF (purple) and [Co**N$_4$H**(MeCN)]$^+$ in MeCN (green) and [Co^{II}**N$_4$H**(MeCN)]$^{2+}$ in MeCN (orange).

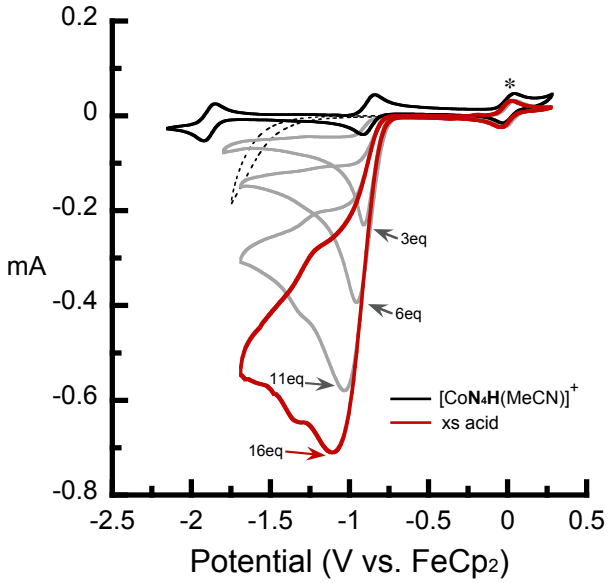

Figure S9. CV of 1 mM [Co**N$_4$H**(MeCN)]$^+$ in MeCN before addition of [H-DMF][OTf] (black). Addition of excess acid to the same solution produced a catalytic wave at a potential near the Co$^{II/I}$ couple for [Co^{III}**N$_4$H**(Br)$_2$]$^+$ (red). The dashed black line is an acid control without added cobalt complex. Conditions: supporting electrolyte = 0.1 M nBu$_4$PF$_6$; glassy carbon used for working and counter electrode; Ag wire used for reference electrode with internal FeCp$_2$ (*). Scan rate = 100 mV/s.

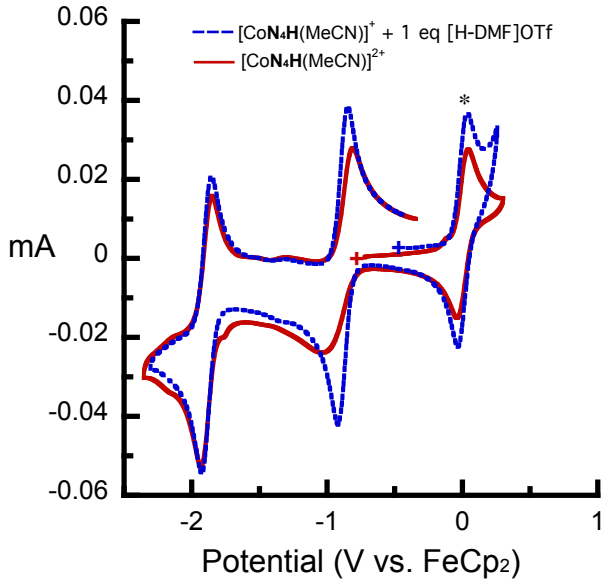

Figure S10. CV of 1 mM [Co**N$_4$H**(MeCN)][BPh$_4$] + 1 equiv [H-DMF][OTf] (dashed blue) and analytically pure 1 mM [Co^{II}**N$_4$H**(MeCN)][OTf][BPh$_4$] (solid red) in MeCN with 0.1 M nBu$_4$NPF$_6$ using a glassy carbon working and counter electrode and a Ag wire reference electrode internally referenced to ferrocene (*). Scan rate = 100 mV/s.

DFT Calculations

optimized coordinates (Å) for [CoN_4]

	X	Y	Z
Co	-0.52659715	-0.00010728	-0.00048919
N	-0.23624953	1.90298070	0.08047210
N	1.27691259	0.00027785	-0.00046092
N	-2.35038303	-0.00043591	0.00045129
N	-0.23542881	-1.90306459	-0.08109992
C	1.96031892	-1.19804541	-0.06833259
C	1.95980245	1.19886198	0.06815208
C	1.02922282	-2.29626495	-0.12973165
C	1.02820285	2.29665652	0.12980887
C	-1.31674895	-2.88046396	-0.12875468
H	-0.98027904	-3.86298515	0.22362826
H	-1.64257624	-3.00359240	-1.17485663
C	-1.31792914	2.88002943	0.12833116
H	-0.98192836	3.86247459	-0.22473582
H	-1.64319645	3.00353939	1.17455362
C	3.35558858	1.21126600	0.07127012
H	3.89747672	2.15024863	0.12638459
C	3.35613010	-1.20984043	-0.07097519
H	3.89844413	-2.14859893	-0.12569549
C	-3.19808086	1.17010004	-0.16740821
H	-3.67587655	1.43630356	0.79923151
H	-4.03323330	0.92584787	-0.84980167
C	1.46740643	3.73371198	0.24019521
H	1.18517517	4.31671255	-0.64695944
H	2.55224708	3.80469632	0.34567972
H	1.01758283	4.22799485	1.11026928
C	-2.49453636	-2.40890984	0.72135321
H	-2.13867308	-2.20927760	1.74094808
H	-3.22953813	-3.22375151	0.78276193
C	-3.19745590	-1.17145786	0.16827324
H	-3.67530039	-1.43767269	-0.79833622
H	-4.03258018	-0.92777491	0.85089673
C	4.05880501	0.00085814	0.00018967
H	5.14457499	0.00109391	0.00031821
C	1.46908651	-3.73317177	-0.23933120
H	1.18484246	-4.31647449	0.64694922
H	2.55419626	-3.80384262	-0.34212522
H	1.02152707	-4.22740419	-1.11064926
C	-2.49595566	2.40777877	-0.72101070
H	-3.23134301	3.22228565	-0.78221610
H	-2.14051819	2.20811546	-1.74075110

optimized coordinates (Å) for [$CoN_4H(MeCN)]^+$

	X	Y	Z
Co	-0.33487604	0.00071690	-0.14576454
N	1.48034593	-0.00097787	-0.15680051
N	-0.03490328	-1.91970151	-0.30249053
N	-0.03130004	1.92079051	-0.30030686
N	-2.15003622	0.00305233	-1.13861891

N	-1.16078976	0.00058258	1.67815937
C	2.15183572	-1.19853548	-0.12303320
C	2.15408160	1.19528098	-0.12173117
C	1.22786633	2.30616673	-0.18771842
C	3.54934804	1.20841799	-0.05478518
C	-2.97098585	1.22577376	-0.94433893
C	1.22355109	-2.30758748	-0.19034153
C	-1.11196812	-2.90739140	-0.34839083
C	3.54708402	-1.21435843	-0.05607493
C	4.24793401	-0.00364847	-0.02249472
C	-2.23098993	-2.50221585	-1.31333756
C	-2.97321903	-1.21844051	-0.94607850
C	-1.10656330	2.91051878	-0.34464874
C	-1.43742438	-0.00185787	2.80480649
C	1.68290971	3.74144552	-0.13468936
C	1.67589448	-3.74378432	-0.13914081
C	-2.22648709	2.50870532	-1.30995168
C	-1.76656359	-0.00591410	4.22742293
H	4.09311438	2.14673964	-0.03380794
H	5.33203568	-0.00468671	0.02372222
H	4.08909000	-2.15371873	-0.03607415
H	-1.84273080	0.00347170	-2.11397499
H	-3.88250243	1.14931082	-1.55541179
H	-3.28416321	1.24871715	0.10582216
H	-0.73494964	-3.89141799	-0.64371211
H	-1.52746174	-3.01353159	0.66512940
H	-1.82710619	-2.42309083	-2.33256992
H	-2.96482680	-3.31745853	-1.33559897
H	-3.28657149	-1.24223464	0.10400648
H	-3.88451977	-1.13951105	-1.55715934
H	-1.52162584	3.01602183	0.66910400
H	-0.72780242	3.89425171	-0.63871391
H	1.44847690	4.27395047	-1.06505014
H	1.20355301	4.28699973	0.68667298
H	2.76189427	3.80791788	0.01404083
H	1.19531372	-4.28956988	0.68135269
H	1.44073131	-4.27459242	-1.07028894
H	2.75471111	-3.81246854	0.00979972
H	-1.82294306	2.43024026	-2.32937165
H	-2.95884933	3.32530624	-1.33096470
H	-2.46035891	0.80897158	4.45871572
H	-2.23492923	-0.95607066	4.50442195
H	-0.85696519	0.12542309	4.82311183

References

(1) Sheldrick, G. M. *Acta. Cryst.* **2008**, *A64*, 112.
(2) Dolomanov O.V., Blake A.J, Champness N.R., Schroder M. (2003). "OLEX: new software for visualization and analysis of extended crystal structures". *J. Appl. Cryst.***36**: 1283–1284
(3) Frisch, M. J.; Trucks, G. W.; Schlegel, H. B.; Scuseria, G. E.; Robb, M. A.; Cheeseman, J. R.; J. A. Montgomery, J.; Vreven, T.; Kudin, K. N.; Burant, J. C.; Millam, J. M.; Iyengar, S. S.; Tomasi, J.; Barone, V.; Mennucci, B.; Cossi, M.; Scalmani, G.; N. Rega; Petersson, G. A.; Nakatsuji, H.; Hada, M.; Ehara, M.; K. Toyota; Fukuda, R.; Hasegawa, J.; Ishida, M.; Nakajima, T.; Honda, Y.; Kitao, O.; Nakai, H.; Klene, M.; Li, X.; Knox, J. E.; Hratchian, H. P.; Cross, J. B.; Bakken, V.; Adamo, C.; Jaramillo, J.; Gomperts, R.; Stratmann, R. E.; Yazyev, O.; Austin, A. J.; Cammi, R.; Pomelli, C.; Ochterski, J. W.; Ayala, P. Y.; Morokuma, K.; Voth, G. A.; Salvador, P.; Dannenberg, J. J.; Zakrzewski, V. G.; Dapprich, S.; Daniels, A. D.; Strain, M. C.; Farkas, O.; Malick, D. K.; Rabuck, A. D.; K. Raghavachari; Foresman, J. B.; Ortiz, J. V.; Cui, Q.; Baboul, A. G.; Clifford, S.; Cioslowski, J.; Stefanov, B. B.; Liu, G.; Liashenko, A.; Piskorz, P.; Komaromi, I.; Martin, R. L.; Fox, D. J.; Keith, T.; Al-Laham, M. A.; Peng, C. Y.; Nanayakkara, A.; Challacombe, M.; Gill, P. M. W.; Johnson, B.; Chen, W.; Wong, M. W.; Gonzalez, C.; Pople, J. A. *Gaussian, Inc.*, Wallingford CT 2004.
(4) a) Seeger, R.; Pople, J. A. *J. Chem. Phys.* **1977**, *66*, 3045. b) Bauernschmitt, R.; Ahlrichs, R. *J. Chem. Phys.* **1996**, *104*, 9047.
(5) a) Ginsberg, A. P. *J. Am. Chem. Soc.* **1980**, *102*, 111. b) Noodleman, L.; Peng, C. Y.; Case, D. A.; Mouesca, J. M. *Coord. Chem. Rev.* **1995**, *144*, 199.
(6) Tinnemans, A. H. A.; Koster, T. P. M.; Thewissen, D. H. M. W.; Mackor, A. *Recl. Trav. Chim. Pay. B.* **1984**, *103*, 288
(7) Che, C.-M.; Mak, S.-T.; Lee, W.-O.; Fung, K.-W.; Mak, T. C. W. *Dalton Trans.* **1988**, 2153
(8) Farr, N. G.; Griesser, H. J. *J. Electron. Spectrosc. Relat. Phenom.* **1989**, *49*, 293-302.
(9) (a) Cabaniss, G. E.; Diamantis, A. A.; Murphy, W. R.; Linton, R. W.; Meyer, T. J. *J. Am. Chem. Soc.* **1985**, *107*, 1845-1853. (b) McCreery, R. L. in *Electroanalytical Chemistry: A Series of Advances*; Bard, A. J., Ed.; Marcel Dekker: New York, 1991; Vol. 17, p 269-273.
(10) The water concentration of the electrolyte solution was measured by Karl-Fischer titration to be 35 ± 4 mM.